DOI: 10.1002/adfm.200600830

Photoelectrical Characteristics of a C/CN_x Multiwalled Nanotube**

By *Kai Xiao*, *Ying Fu*, *Yunqi Liu*,* *Gui Yu*, *Jin Zhai*, *Lei Jiang*, *Wenping Hu*,* *Zhigang Shuai*, *Yi Luo*,* and *Daoben Zhu**

A nanotube diode fabricated from a single C/CN_x multiwalled nanotube exhibits a large photocurrent and a large photovoltage under illumination. The current–voltage (*I–V*) characteristics of the diode indicate a clear rectification effect. By comparing the *I–V* characteristics of C, CN_x, and C/CN_x nanotube diodes, we show that the rectifying characteristics of the C/CN_x diode arises from the molecular junction formed at the C/CN_x interface where the C and CN_x segments are chemically bonded. External radiation photochemically generates electrons and holes in the C/CN_x nanotube, producing a large photocurrent because of the influence of the strong electric field in the vicinity of the C/CN_x junction. These unique photoresponsive characteristics of C/CN_x nanotube junction diodes points to potential applications such as photovoltaic devices and photodiodes.

1. Introduction

Since the first discovery of carbon nanotubes (CNTs) in the 1990s, there has been a lot of interest in the possibility of connecting segments of different types of CNTs to form novel building blocks for nanoscale electronic devices and circuits.[1–5] CNTs with different electrical properties can be connected via pentagon–heptagon pair-defects or other types of defects.[6–11] There have also been reports of crossed nanotube junctions without the formation of chemical bonds,[4] as well as more complex structures such as "T" or "Y" junctions.[5] Rectification effects have been observed in the current–voltage (*I–V*) characteristics measured across many intra-tube junctions.[3,4,6,12] However, not much attention has been focused on the use of CNTs in photoelectrical devices. The photoconductivities of single-walled CNTs (SWCNTs) have been recently measured under near-IR,[13] UV,[14] and IR-laser illumination.[15] Furthermore, the emission of polarized light has been observed in CNT field-effect transistors.[16]

[*] Prof. Y. Q. Liu, Prof. W. P. Hu, Prof. D. B. Zhu, Dr. K. Xiao, Dr. G. Yu, Dr. J. Zhai, Prof. L. Jiang, Prof. Z. G. Shuai
Beijing National Laboratory for Molecular Sciences, Institute of Chemistry
Chinese Academy of Sciences
Beijing 100080 (P.R. China)
E-mail: liuyq@mail.iccas.ac.cn; huwp@iccas.ac.cn; zhudb@iccas.ac.cn
Prof. Y. Luo, Prof. Y. Fu
Department of Theoretical Chemistry
Royal Institute of Technology
AlbaNova S-106 91, Stockholm (Sweden)
E-mail: luo@kth.se

[**] The authors acknowledge partial financial support from NSFC (90 206 049, 20 472 089, 20 421 101, 20 404 013, 20 527 001, 20 573 115, 50 673 093, 60 671 047), MOST, and CAS. YL acknowledges support from the Swedish Research Council and the Carl Trygger Foundation.

CNT p–n junctions and other junction diodes showing optoelectronic effects have been fabricated by electrostatically defining separate sections on a nanotube, using crossed-wire geometries, and by the modulated chemical doping of nanotube sections. These CNT junctions are excellent candidates for optoelectronic devices with a much reduced dimensionality. Here, we demonstrate a junction-type photoconductive diode based on a single C/CN_x multiwalled nanotube (MWCNT). We also propose a novel phototransistor device wherein the electrical current can be tuned by the intensity of the external radiation, unlike conventional electronic devices, which are controlled by electric or magnetic fields.[17,18] Our results suggest that the MWCNT junctions could potentially be useful for photosensing applications such as in photovoltaic devices and photodiodes.

2. Results and Discussion

The C/CN_x MWCNT device is schematically shown in Figure 1c. Typical *I–V* characteristics of the device measured in the dark and under illumination are shown in Figure 2a. Figure 2 shows two distinct features of this device: i) a large photocurrent and a large photovoltage are obtained under white light illumination, and ii) the *I–V* characteristics are asymmetric with respect to the polarity of the bias, thus exhibiting a rectifying effect.

Figure 3 schematically depicts the band structure of the open-circuit C/CN_x photoconductive diode studied here. At first glance, the junction appears to act as a macroscopic Schottky junction since it is formed between a metallic C segment and a semiconducting CN_x section. The contacts between the C/CN_x MWCNT and the two electrodes are expected to be ohmic, as indicated by the linear *I–V* characteristics of the C- and CN_x-CNT-based diodes. The C- and CN_x-CNTs have been determined to be metallic and n-type semiconducting, respectively.[6,19] It is worth noting that the C and CN_x segments are

InterScience®
© 2007 WILEY-VCH Verlag GmbH & Co. KGaA, Weinheim

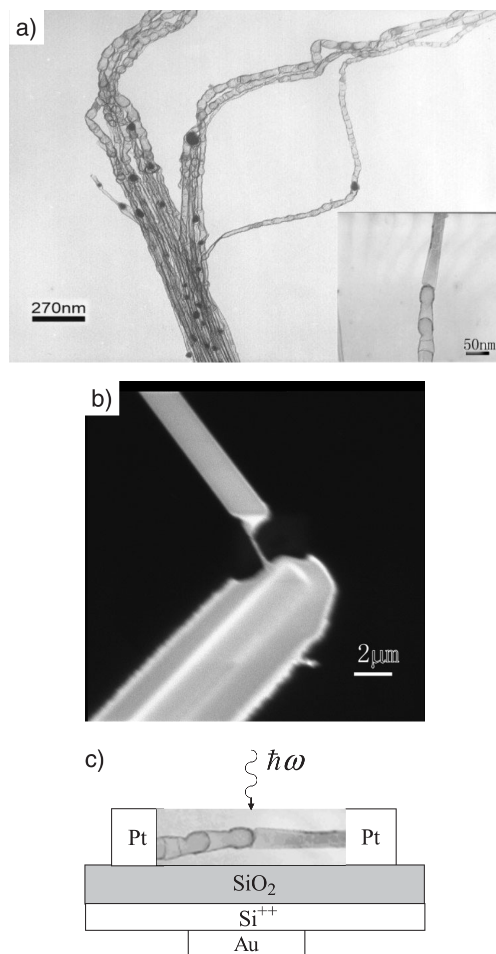

Figure 1. a) Typical transmission electron microscopy image of a bundle of C/CN_x MWCNTs. The inset shows a single C/CN_x MWCNT. b) Scanning electron microscopy image of the connections between the C/CN_x MWCNT and the electrodes. c) Schematic structure showing a device based on a single C/CN_x MWCNT; the C/CN_x MWCNT is about 2.0 µm long and has a diameter of about 50 nm.

linked by chemical bonds, and thus at the junction, the band structures of the two segments are expected to be combined to form a potential barrier. From a microscopic point of view, the actual junction thus resembles a heterojunction, or more precisely a molecular junction. In this picture, the metallic C segment serves as a metal electrode, whereas the CN_x segment acts as a semiconducting electrode. The C–CN_x junction behaves like a large molecule bridging the two electrodes.

The observed photocurrent and photovoltage are related to the creation of electron–hole pairs after photon absorption. The properties of the electron–hole pairs depend on their spatial location along the C/CN_x MWCNT. Excitons are expected to form in the bulk sections of the MWCNT because of the strong 2D quantum confinement, and thus a much enhanced Coulombic electron–hole coupling is observed in the cross-section of the MWCNT.[20] Consequently, the optical absorption probability is increased, the drift-diffusion velocity of the carriers becomes larger, and the carrier relaxation time becomes longer.[15,21,22] On the other hand, the photogenerated electrons and holes in the vicinity of the C–CN_x junction are directly driven by the strong electric field across the junction (see shadowed area in Fig. 3), thus generating the strong observed photocurrent. Notably, the C/CN_x MWCNT has a very high carrier mobility of about 10^3 $cm^2\,V^{-1}\,s^{-1}$.[17] The photocurrent and open-circuit photovoltage of the C/CN_x MWCNT device are plotted as functions of the optical excitation power in Figure 2b. The monotonic correlations between the photocurrent/photovoltage and the optical power is consistent with the results shown in Figure 2a. Specifically, these results corroborate the effective electron–hole separation in the C–CN_x junction and the efficient charge transport along the MWCNT.

Electron–hole pairs are generated in the C/CN_x MWCNT upon illumination with light. The photocurrent is obtained when an external bias is applied across the C/CN_x MWCNT. In the case of an open circuit, a photovoltage $V_{\hbar\omega}$ is generated due to the extra photogenerated carriers in the C/CN_x MWCNT. To quantitatively describe the optoelectronic properties of the C/CN_x MWCNT, we model the MWCNT as a long effective-medium quantum wire with a cross-section defined by its radius. Furthermore, we assume that the incident illumination is not polarized. Upon positioning the C/CN_x MWCNT along the z-axis, the energy structures of both the conduction-band electrons and the valence-band holes consist of discrete levels in the xy-plane, which are denoted as $[E_i, \psi_i(x,y)]$, where E_i and $\psi_i(x,y)$ are the eigenvalue and eigenfunction of state i, respectively. Along the z-axis, the wave function is in the form of a plane wave e^{ikz}.[23] Knowing the eigenvalues and eigenfunctions describing the active electrons, the interaction between the incident radiation and the electron is given by

$$\frac{e}{m_0}\mathbf{A}\bullet\mathbf{p} = \frac{e}{m_0}A_x p_x \tag{1}$$

for the present device configuration, where the radiation propagates along the y-direction so that its field vector $\boldsymbol{A}$ is decomposed into x- and z-components as (see Fig. 1c)

$$\mathbf{A} = A_x\boldsymbol{x}_0 + A_z\boldsymbol{z}_0 \tag{2}$$

Here e is the elementary charge, m_0 is the electron rest mass, and $\boldsymbol{p}$ is the momentum of the electron; $\boldsymbol{x}_0$ and $\boldsymbol{z}_0$ are unit vectors in the x- and z-directions, respectively. It is easy to show that

$$P_{ij,kq} = \left\langle \psi_i(x,y)e^{ikz}|\mathbf{A}\bullet\mathbf{p}|\psi_j(x,y)e^{iqz}\right\rangle = \delta_{k,q}\iint dxdy\psi_i^*(x,y)\frac{\partial\psi_j(x,y)}{\partial x} \tag{3}$$

where $\delta_{k,q}$ represents the vertical optical transition because of the small momentum of light. The averaged transition probability per unit time is

$$\frac{2\pi}{\hbar}\frac{e^2|P_{ij,k}|^2}{m_0^2}\frac{\Gamma}{\Omega_{ij,k}^2+\Gamma^2} \tag{4}$$

where

$$\Omega_{ij,k} = E_i + \frac{\hbar^2k^2}{2m_e^*} - E_j + \frac{\hbar^2k^2}{2m_h^*} - \hbar\omega \tag{5}$$

 © 2007 WILEY-VCH Verlag GmbH & Co. KGaA, Weinheim

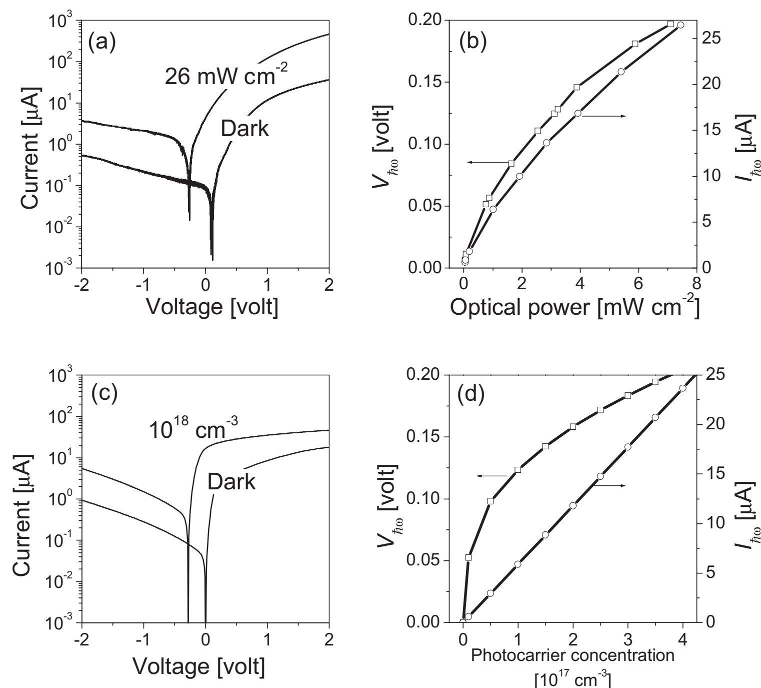

Figure 2. a) Typical *I–V* characteristics of a single C/CN_x MWCNT in the dark and under external illumination (26 mW cm^{-2}). b) Photovoltage $V_{\hbar\omega}$ (◇) and photocurrent $I_{\hbar\omega}$ (○) as functions of the optical excitation power. c) Theoretical calculation of the *I–V* characteristics of a single C/CN_x MWCNT in the dark and under illumination (assuming a photocarrier concentration of 10^{18} cm^{-3}). d) Theoretical predictions of the photovoltage $V_{\hbar\omega}$ (◇) and photocurrent $I_{\hbar\omega}$ (○) as functions of the photocarrier concentration (which is proportional to the optical excitation power). The solid lines are shown only as guides to the eye.

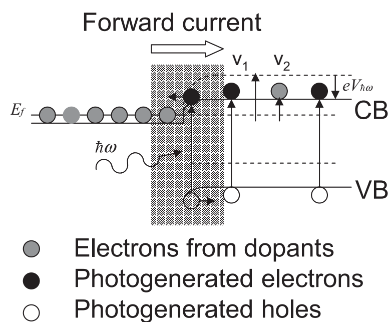

Figure 3. Schematic depiction of the band structure of the C/CN_x MWCNT photoconductive diode. CB denotes the conduction band edge, whereas VB is the valence band edge. At the junction, the bands of the two segments are combined through chemical bonds to form a potential barrier.

m_e^* and m_h^* are the effective masses of the conduction-band electrons and valence-band holes, respectively, Γ is the relaxation energy of the excited states, and $\hbar\omega$ is the photon energy of the incident radiation.

On the other hand, the cross-section of the MWCNT is effectively quite large and thus we can neglect the discrete characteristics of the energy sublevels in the *xy*-plane by dropping the subscripts *i* and *j*. We further take into account the fact that the illuminating radiation is not polarized, and therefore the optical transition probability becomes

$$\frac{\pi e^2|p|^2 S}{\hbar m_0^2 \varepsilon c}\frac{\Gamma}{\Omega_k^2+\Gamma^2} \tag{6}$$

where *S* is the optical excitation power of the incident radiation, *c* is the speed of light, ε is the permittivity of the material, and

$$p=\int dx\int dy\psi_i^*(x,y)\frac{\partial\psi_j(x,y)}{\partial x} \tag{7}$$

is the matrix element of momentum. The concentration of photogenerated carriers in the C/CN_x MWCNT becomes

$$n(\hbar\omega)=\frac{\pi e^2|p|^2 S}{\hbar m_0^2 \varepsilon c}\int[1-f_e(k)]f_h(k)\frac{dk/\pi}{\Omega_k^2+\Gamma^2} \tag{8}$$

where $f_e(k)$ and $f_h(k)$ are the occupations of the conduction- and valence-band states *k*, respectively. The quantity $2dk/2\pi$ represents the number of electron states in the *k*-space volume of *dk*. The total photogenerated carrier concentration is $n'=\int n(\hbar\omega)d\omega$. Note that in the above expression, the relationship between *S* and $\hbar\omega$ is determined by the light source used.

It is worth noting that $f_e(k)$ and $f_h(k)$ are modified upon external illumination due to the generation of photocarriers, and thus in general, the correlation between the photocarrier concentration and the optical excitation power is not linear. At a quasi-thermal equilibrium state,

$$f_e(k)=\frac{1}{1+\exp\left[\left(E_i+\frac{\hbar^2k^2}{2m_e^*}-E_f\right)/k_BT\right]} \tag{9}$$

and thus the carrier distribution function $f_e(k)$ can be correlated to the photogenerated carrier concentration as

$$n+n'=\int f_e(k)\frac{dk}{\pi} \tag{10}$$

where *n* is the concentration of free electrons in the C/CN_x MWCNT without light illumination. Here, we have assumed that the photogenerated carriers instantaneously reach thermal equilibrium with the MWCNT lattice via various relaxation processes.

In physical terms, the incidence of light on the C/CN_x nanotube leads to the generation of electron–hole pairs. Since the dark current in the C/CN_x nanotube is much lower than the photocurrent, the concentration of free electrons is expected to be small, i.e., $f_e(k)\ll 1.0$ before illumination. If the optical excitation power is low so that under illumination, $f_e(k)$ is still far less than 1.0, Equation 8 becomes

$$n(\hbar\omega)\approx\frac{\pi e^2|p|^2 S}{\hbar m_0^2 \varepsilon c}\int\frac{dk/\pi}{\Omega^2+\Gamma^2}\propto S \tag{11}$$

and thus the concentration of photocarriers in the C/CN_x nanotube is proportional to the optical excitation power *S*. Therefore, when the excitation power is low, we expect a linear rela-

© 2007 WILEY-VCH Verlag GmbH & Co. KGaA, Weinheim

tionship between the optical excitation power and the concentration of photocarriers.

When the optical excitation power is significantly increased, photocarrier generation is determined by the Pauli exclusion principle, which states that the initial electron state should be occupied (i.e., $f_h(k)>0$) and the final electron state should be empty (i.e., $f_e(k)<1$). With increased carrier concentration in the conduction band, the corresponding quasi Fermi level also increases so that for the same state k, the value of $[1-f_e(k)]$ decreases. This implies a decrease of the optical excitation rate at k. The exact relationship between the optical excitation power S and the photocarriers is therefore determined jointly by Equations 8 and 10.

To theoretically model the experimentally observed relationships between the photocurrent, the open-circuit photovoltage $V_{\hbar\omega}$ (Fig. 3), and S, we divide the carrier transport along the z-direction into two parts. Electron transport through the C and CN_x segments is described by a drift-diffusion mobility model with $i=-en\mu$, where i is the current, μ is the drift-diffusion mobility of electrons, and n is the carrier concentration. The values of μ and n in the C and CN_x segments are obtained by fitting the experimental I–V curves in Figure 2a and b with the theoretical expressions. Transport through the C–CN_x junction (Fig. 3) is modeled by the 1D Schrödinger equation

$$\left[\frac{-\hbar^2}{2m_e^*}\frac{d^2}{dz^2}+V(z)\right]\psi(z)=E\psi(z) \tag{12}$$

where m_e^* is the effective mass of the active electrons. In the numerical calculations, we set $m_e^*=0.5\,m_0$. $V(z)$ is the potential energy including the band offsets across the C–CN_x junction. This term also contains the Coulomb potential $-e\phi(z)$ arising from ionized impurities described by the doping profile $N_D(z)$ and the free carrier distribution $n(z)$

$$\frac{d}{dz}\left[\varepsilon(z)\frac{d\phi(z)}{dz}\right]=-e[n(z)-N_D(z)] \tag{13}$$

The external bias and the photovoltage are included in the boundary conditions of the above Poisson equation. The carrier distribution $n(z)$ is coupled to the Schrödinger equation via

$$n(z)=\frac{m_e^*k_BT}{2\hbar^2\pi}\sum_E|\psi_E(z)|^2\ln\left[1+\exp\left(\frac{E_f-E}{k_BT}\right)\right] \tag{14}$$

where E_f is the quasi Fermi level of free electrons in the C/CN_x MWCNT. It is assumed in the above formulations that the carrier transport along the z-axis is rather small so that the equilibrium status of the electrons in the C/CN_x MWCNT is only perturbed by the external voltage. E_f is always a valid physical quantity.

At steady state, we consider carrier transport from the left side of the C–CN_x junction in terms of an incoming plane wave from the left side, a reflection wave from the junction back to the left side, and a transmission wave through the junction:

$$\psi_k(z)=\begin{cases}e^{ikz}+r_ke^{-ikz} if\ z>w\\ t_ke^{iqz} if\ z<0\end{cases} \tag{15}$$

where w is the effective thickness of the junction, $z<0$ denotes the left side of the junction, $z>w$ denotes the right side of the junction, and t_k and r_k are reflection and transmission rates, respectively.

$$\frac{\hbar k^2}{2m_e^*}=\frac{\hbar^2q^2}{2m_e^*}+\Delta V_{CB} \tag{16}$$

where ΔV_{CB} is the change in the conduction band-edge of the C–CN_x junction due to chemical bonding, as well as the application of an external voltage and illumination. In the above equation, $\boldsymbol{k}$ is the wave vector of the incoming plane wave along the z-axis. The value of this vector is determined by the available states on the left side of the junction. In numerical calculations, the C segment is modeled as having a high free-electron concentration of 10^{21} cm^{-3}. The current of the transmission wave is calculated quantum mechanically as

$$i_k=\frac{e}{2im_e*}\left(\psi_k*\frac{\partial\psi_k}{\partial z}-\psi_k\frac{\partial\psi_k*}{\partial z}\right) \tag{17}$$

It is easy to show that

$$i_k=\frac{ek\left(1-|r_k|^2\right)}{m_e^*}=\frac{eq|t_k|^2}{m_e^*} \tag{18}$$

Thus that the total current through the junction is

$$i=\int i_kf_e(k)\frac{dk}{\pi} \tag{19}$$

An analogous approach is used to model electron conduction from the right to the left side of the junction. The total current across the junction is then coupled to the drift-diffusion current in the C and CN_x segments.

Figure 2c and d shows the calculated relationships of the photovoltage and photocurrent with the optical power derived assuming carrier concentrations of 10^{17} and 10^{18} cm^{-3} for the CN_x segment in the dark and under 26 mW cm^{-2} illumination, respectively. We observe very good agreement between the experimental results and the theoretical model if we assume a linear relationship between the optical power and the photocarrier concentration. The numerically calculated photovoltage $V_{\hbar\omega}$ is 0.28 V, almost the same as the experimental value. The experimentally observed nonlinear relationship between the photocurrent and the optical excitation power can be understood based on the filling of the conduction and valence bands by photogenerated electrons and holes. It is worth noting that in the numerical calculations we have assumed a total carrier concentration of 10^{18} cm^{-3} in the CN_x segment under illumination to model the optical transitions (Γ, introduced in Eq. 4, is therefore not used). Furthermore, the theoretical value of the current in Figure 2d is largely determined by the carrier conduction in the CN_x segment based on the mobility model that best fits the experimental data. The most notable features are the value of $V_{\hbar\omega}$ and its nonlinear dependence on the external excitation power, as shown in Figure 2b and d.

Another important characteristic notable in the I–V plots is the left-shift of the current dip after illumination, which is a direct result of the generated photovoltage, as shown in Figure 3. Before illumination, a barrier of v_1 needs to be overcome for

© 2007 WILEY-VCH Verlag GmbH & Co. KGaA, Weinheim

the injection of electrons from the C segment to the CN_x segment. This barrier becomes $v_2 = v_1 - V_{\hbar\omega}$ after illumination, where $V_{\hbar\omega}$ is the photovoltage.

The photocurrent of the C/CN_x MWCNT device also depends on the wavelength of the incident light. The maximum photocurrent values are observed for red light in the 650–750 nm range, as shown in Figure 4a. Figure 4b plots the photoresponse as a function of time as the light source is switched on and off. Depending on the optical excitation power, the conductivity of the C/CN_x MWCNT can be reversibly tuned by three to four orders of magnitude so that the device works as a nanometer-scale photoswitcher.

In order to further understand the electron-transport properties of the C/CN_x MWCNT, a back-side Au substrate has been connected as a gate electrode, as shown in Figure 1c, converting the diode device into a three-terminal transistor. The electrical properties of the transistor are very similar to devices described in the literature.[17] However, the resistance of the current C/CN_x MWCNT device can be modulated significantly by changing the optical excitation power. This photoelectric gain suggests that optical gating (analogous to conventional electrical or magnetic gating) is operational in our C/CN_x MWCNT, resulting in a light-controlled "photo-field-effect transistor".

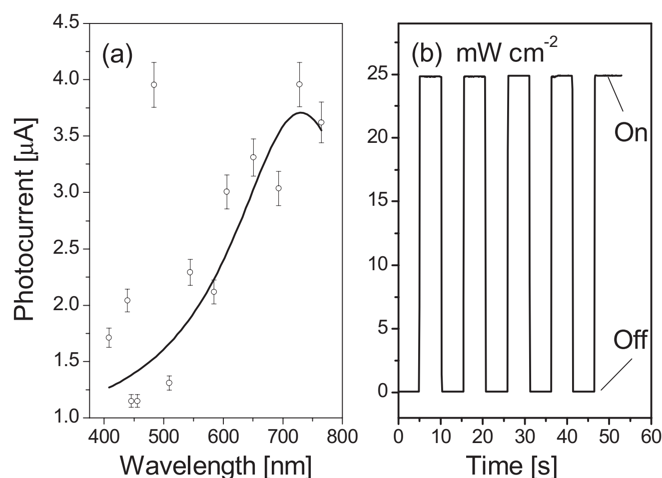

Figure 4. a) The photocurrent spectrum of the C/CN_x MWCNT at zero external bias. The intensities at different wavelengths have all been normalized to 1 mW cm^{-2}. b) Reversible switching of the C/CN_x MWCNT between low- and high-conductivity states as a 5 mW cm^{-2} white light source is turned on and off. No bias voltage is applied during the measurements.

3. Conclusions

We have demonstrated that a large photocurrent and photovoltage can be induced in a C/CN_x MWCNT device by external radiation. Furthermore, the *I–V* characteristics of the device and the observed photocurrent exhibit clear rectification effects. The results are explained by the formation of a molecular junction between the C and CN_x segments in the device. A strong built-in electric field exists across the C–CN_x junction, which effectively drives the photogenerated electrons and holes, generating the large observed photocurrent. The characteristic photoresponse of the C/CN_x MWCNT clearly shows its potential in photosensing applications such as photovoltaic devices and photodiodes (including the light-controlled transistor reported in this work).

4. Experimental

The C/CN_x MWCNT used in this work was composed of C and CN_x segments [6]: the CN_x segment was bamboo-like, whereas the C segment was cylindrical and straight. The cross-sectional diameter of the nanotube ranged between 50 and 70 nm (Fig. 1a). The photoconductive device based on this single C/CN_x nanotube was fabricated as described previously in the literature [17]. Field-emission scanning electron microscopy (JOEL JSM-6301F) was used to obtain detailed images of the C/CN_x MWCNT device (Fig. 1b). A 500 W xenon lamp was used as the white light source along with a quartz optical fiber. Monochromatic light sources were obtained by using the appropriate optical filters. The photocurrent measurements were carried out on a model 600 voltammetric analyzer (CH instruments, USA). The intensities of the incident beams were controlled using power and energy meters (Model 372, Scienteck). IR light from the xenon lamp was filtered using a Toshiba IRA-25s filter (Japan) to prevent the heating of the electrodes.

Received: September 10, 2006
Revised: February 24, 2007
Published online: August 21, 2007

[1] A. Bachtold, P. Hadley, T. Nakanishi, C. Dekker, *Science* **2001**, *294*, 1317.
[2] Y. Huang, X. F. Duan, Y. Cui, L. J. Lauhon, K. H. Kim, C. M. Lieber, *Science* **2001**, *294*, 1313.
[3] Z. Yao, W. Ch. Postma, L. Balents, C. Dekker, *Nature* **1999**, *402*, 273.
[4] W. Ch. Postma, M. de Jonge, Z. Yao, *Phys. Rev. B: Condens. Matter* **2000**, *62*, R10 653.
[5] A. N. Andriotis, M. Menon, D. Srivastava, L. Chernozatonskii, *Appl. Phys. Lett.* **2001**, *79*, 266.
[6] P. A. Hu, K. Xiao, Y. Q. Liu, G. Yu, X. B. Wang, L. Fu, G. L. Cui, D. B. Zhu, *Appl. Phys. Lett.* **2004**, *84*, 4932.
[7] M. Ouyang, J. L. Huang, C. L. Cheung, C. M. Lieber, *Science* **2001**, *291*, 97.
[8] D. A. Stewart, F. Léonard, *Phys. Rev. Lett.* **2004**, *93*, 10 7401.
[9] J. U. Lee, P. P. Gipp, C. M. Heller, *Appl. Phys. Lett.* **2004**, *85*, 145.
[10] J. U. Lee, *Appl. Phys. Lett.* **2005**, *87*, 073 101.
[11] D. A. Stewart, F. Léonard, *Nano Lett.* **2005**, *5*, 219.
[12] P. G. Collins, A. Zettl, H. Bando, A. Thess, R. E. Smalley, *Science* **1997**, *278*, 100.
[13] I. A. Levitsky, W. B. Euler, *Appl. Phys. Lett.* **2003**, *83*, 1857.
[14] M. Shim, G. P. Siddons, *Appl. Phys. Lett.* **2003**, *83*, 3564.
[15] M. Freitag, Y. Martin, J. A. Misewich, R. Martel, Ph. Avouris, *Nano Lett.* **2003**, *3*, 1067.
[16] J. A. Misewich, R. Martel, Ph. Avouris, J. C. Tsang, S. Heinze, J. Tersoff, *Science* **2003**, *300*, 783.
[17] K. Xiao, Y. Q. Liu, P. A. Hu, G. Yu, L. Fu, D. B. Zhu, *Appl. Phys. Lett.* **2003**, *83*, 4824.
[18] R. N. Gurzhi, A. N. Kalinenko, A. I. Kopeliovich, A. V. Yanovsky, E. N. Bogachek, U. Landman, *Appl. Phys. Lett.* **2003**, *83*, 4577.
[19] K. Xiao, Y. Q. Liu, P. A. Hu, G. Yu, Y. M. Sun, D. B. Zhu, *J. Am. Chem. Soc.* **2005**, *127*, 8614.
[20] E. J. Mele, *Phys. Rev. B: Condens. Matter* **2000**, *61*, 7669.
[21] Ph. Avouris, *MRS Bull.* **2004**, *29*, 403.
[22] V. Perebeinos, J. Tersoff, Ph. Avouris, *Phys. Rev. Lett.* **2004**, *92*, 257 402.
[23] A. Goldberg, H. M. Schey, J. L. Schwartz, *Amer. J. Phys.* **1967**, *35*, 177.

© 2007 WILEY-VCH Verlag GmbH & Co. KGaA, Weinheim